THE JOURNAL OF PHYSICAL CHEMISTRY B

Article

pubs.acs.org/JPCB

Study of the Structural Role of Gallium and Aluminum in 45S5 Bioactive Glasses by Molecular Dynamics Simulations

Gianluca Malavasi, Alfonso Pedone,* and Maria Cristina Menziani

Department of Chemical and Geological Sciences, University of Modena and Reggio Emilia, via G. Campi 183, 41125 Modena, Italy

ABSTRACT: The structural properties of phosphosilicate glasses based on the 45S5 Bioglass doped with gallium and aluminum ($46.2SiO_2{\cdot}24.3Na_2O{\cdot}26.9CaO{\cdot}2.6P_2O_5{\cdot}1.0X_2O_3$, X = Ga or Al) are investigated by means of classical molecular dynamics simulations. Structural features of the two compositions are compared with those of the original 45S5 Bioglass in order to relate them to the different known bioactivities of these materials. Differences in the coordination environments of Ga and Al, network connectivity, and ion aggregation reveal a microscopic model of these glasses which supports the interpretation of the experimental data and provides new insight into the different biological behaviors of Ga- and Al-containing phosphosilicate glasses. Although Ga is found predominantly in a 4-fold coordination environment, small amounts of 5- and 6-fold coordinated atoms have been detected depending on the interatomic potential model employed. This suggests its possible intermediate role in phosphosilicate glasses. On the contrary, Al plays a network former role and leads to glasses with a more polymerized structure. Interestingly, the results show an increased propensity for aggregation of the Ca^{2+} and PO_4^{3-} ions in the Al-containing phosphosilicate glasses with respect to the Ga-containing ones. This leads to insoluble calcium-phosphate-rich regions not detected in the bioactive glasses.

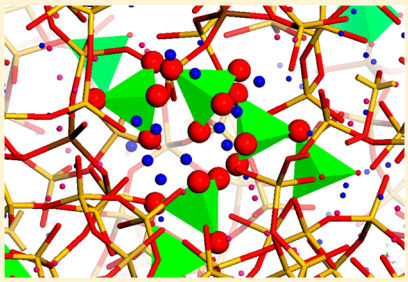

INTRODUCTION

Bioactive glasses represent an important class of biomaterials widely employed in bone repair and replacement, in that they spontaneously bond and integrate with living tissues thanks to the formation on their surface of a layer of biologically active hydroxyl-carbonate-apatite (HCA), once in contact with biological fluids. The first glass showing bioactivity, discovered by Hench in the early 1970s, was a phosphosilicate glass containing sodium and calcium oxides, and it is known as the 45S5 Bioglass.[1] Since then, a great variety of glasses and glass-ceramics of different chemical composition have been prepared and extensively studied in order to obtain new materials with improved chemical, mechanical, and biological features tailored for specific clinical applications.[2−7]

Among the large variety of inorganic dopants introduced in the glass composition, Ga_2O_3 represents a quite interesting and promising agent due to its diverse array of reported therapeutic activities.[8] In fact, it has been demonstrated that Ga^{3+} is an efficient agent approved by Food and Drug Administration (FDA) for the cure of hypercalcemia associated with bone tumor metastasis. Moreover, once released into the physiological environment, Ga^{3+} can disrupt the Fe^{3+} metabolism of many infecting bacteria unable to differentiate between the two trivalent cations.[9] In fact, the substitution of iron, a redox active species essential in electron transport and oxidative stress, with gallium, redox inactive, increases the vulnerability of these microorganisms. Thus, in the recent years, there has been a growing interest in combining Ga^{3+} with biodegradable materials to prevent bacterial colonization after surgery, which would otherwise require the systematic administration of antibiotics.[10]

Valappin et al.[9] synthesized Ga^{3+}-containing phosphate glasses and successfully tested their bactericidal activity, showing that the high phosphate and sodium content warrant for fast glass dissolution and the Ga^{3+} delivery inhibits the growth of *P. aeruginosa*.

However, fully biodegradable Ga-phosphate glasses can lead to a very high concentration of Ga ions in aqueous solution, up to 20−80 ppm as a function of glass composition after a few hours of soaking. Since the toxic limit of Ga^{3+} ions in blood plasma is 14 ppm,[8] different Ga-delivery systems have been investigated very recently.

Mouriño et al.[11] prepared and characterized gallium releasing 3D scaffolds for bone tissue engineering made of the 45S5 Bioglass coated with a 3-D alginate polymer used as a vehicle for Ga^{3+} delivery, whereas Franchini et al.[12] incorporated Ga ions in phosphosilicate bioactive glasses with the aim of combining the antimicrobial properties of Ga^{3+} ions along with the ability of Bioglass 45S5 to form a bond with the bone in living system without toxic effects. This ability was later demonstrated by Shruti et al.[13]

Therefore, phosphosilicate glasses are better suited (with respect to phosphate glasses) to be used as coatings for metallic prosthesis in order to obtain osteointegration of the implant with low inflammatory risks.

However, since bioactivity greatly depends on the release of ionic species in the surrounding physiological environment, it is critical to obtain a very accurate picture of the structural

Received: January 22, 2013
Revised: March 11, 2013
Published: March 20, 2013

dx.doi.org/10.1021/jp400721g | *J. Phys. Chem. B* 2013, 117, 4142−4150

organization of the constituting components of the glass in order to be able to develop better biomaterials with a greater focus on end-user application requirements, reducing development costs, and speeding up the time to market.

The structural role of Ga^{3+} in the network of a silicate glass has always been considered to be similar to that of Al^{3+} in view of the ability of both ions to assume tetrahedral and octahedral coordination geometries toward oxygen, both in crystalline compounds and in glasses.[14−17]

However, recent results reported in the literature seem to disprove this assumption. In fact, in contrast with the inhibitory effect on the formation of bioactive HCA exerted by a small amount (1.75 mol %) of Al_2O_3 added to the 45S5 glass and A/W glass−ceramic,[18] Franchini et al.[17] showed that 1.6 mol % of Ga_2O_3 added to Bioglass 45S5 does not inhibit the formation of HCA after 1 day of immersion in simulated body fluid (SBF).[19,20] Furthermore, 3.5 mol % of Ga_2O_3 does not prevent HCA formation after 15 days of glass immersion in SBF.

Ambiguities in the interpretation of experimental results can be clarified by molecular dynamics (MD) simulations which provide a detailed description of the glass structure and of the structural role of its components. Several MD studies focused on the structure of the original 45S5 Bioglass[21−25] and of other bioactive glasses have been carried out in the past.[25−32] Other MD studies have been carried out to investigate the role of Al in highly durable silicate glasses[33,34] and multicomponent aluminosilicate glasses,[35,36] but to our knowledge, no computational studies are present in the literature for multicomponent glasses containing gallium.

In the present work, the structural role of Ga and Al ions added to the 45S5 Bioglass will be disclosed by means of classical molecular dynamics simulations with the aim of better understanding their effect on the structure of the parent Bioglass and their different biological behavior.

Computational Procedure. MD simulations were performed by means of the DL_POLY package.[37] Structural models of glasses with composition $46.2SiO_2{\cdot}24.3Na_2O{\cdot}26.9CaO{\cdot}2.6P_2O_5{\cdot}xX_2O_3$ (x = 0 named BG; x = 1.0 and X = Ga named GBG; and x = 1.0 and X = Al named ABG hereafter) were generated by means of the melt quench approach.[38]

Two interatomic potential models, that is, the rigid ionic model (RI) and the core−shell model (SM) have been used. In the framework of the RI model, the pairwise interatomic potentials developed by Pedone et al.[38−40] were used to model the O−O, Si−O, Na−O, Ca−O, and P−O pair interactions whose parameters are reported in Table 1. This assumes partial charges on the ionic core to handle the partial covalency of silicate systems and is given by the combination of a long-range Coulomb potential with a short-range Morse function, and a repulsive contribution of the form B/r^{12}, necessary to prevent atomic collapse at high temperature and pressure:

$$U_{ij}(r) = \frac{z_i z_j e^2}{r} + D_{ij}[\{1 - e^{-a_{ij}(r-r_0)}\}^2 - 1] + \frac{B_{ij}}{r^{12}} \quad (1)$$

Instead, a Buchingham function has been used to model the Ga−O and Al−O short-range interactions (Table 1):

$$U_{ij}(r) = \frac{z_i z_j e^2}{r} + A_{ij} e^{-r/\rho_{ij}} - \frac{C_{ij}}{r^6} + \frac{B_{ij}}{r^{12}} \quad (2)$$

However, while the Al−O interatomic potential parameters have been previously employed to simulate aluminosilicate glasses,[33] the Ga−O parameters have been derived here for the first time by fitting to the crystal structures of two gallium silicates, $NaGaSiO_4$ and $NaCaGaSi_2O_7$, using the GULP code[41] with all the other interaction parameters kept fixed at the original values.

Table 1. Rigid Ionic Model: Morse and Buckingham Interatomic Potential Parameters Used for Molecular Dynamics Simulations

Morse Parameters				
atom pairs	D_{ij} (eV)	a_{ij} (Å^{-2})	r_0 (Å)	B_{ij} (eV Å^{12})
$O^{-1.2}$–$O^{-1.2}$	0.042395	1.379316	3.618701	22.0
$Si^{+2.4}$–$O^{-1.2}$	0.340554	2.006700	2.100000	1.0
$Na^{+0.6}$–$O^{-1.2}$	0.023363	1.763867	3.006315	5.0
$Ca^{+1.2}$–$O^{-1.2}$	0.030211	2.241334	2.923245	5.0
$P^{+3.0}$–$O^{-1.2}$	0.831326	2.585833	1.800790	1.0
Buckingham Parameters				
atom pairs	A_{ij} (eV)	ρ_{ij} (Å^{-2})	C_{ij} (eV Å^6)	B_{ij} (eV Å^{12})
$Ga^{+1.8}$–$O^{-1.2}$	10447.35	0.2080	41.938	15.0
$Al^{+1.8}$–$O^{-1.2}$	12201.41	0.1956	31.997	15.0

The $NaGaSiO_4$ and $NaCaGaSi_2O_7$ crystals have been chosen, since they are the crystal phases obtained after crystallization of the $46.2SiO_2{\cdot}24.3Na_2O{\cdot}26.9CaO{\cdot}2.6P_2O_5{\cdot}3.5Ga_2O_3$ glass; therefore, the glasses under study should bear structural features similar to those of those crystals.[42]

Although it is generally known that the medium range structure of silicate glasses is better reproduced through the shell-model potentials rather than the rigid ionic one,[43] we first decided to employ the latter because it allows the investigation, in an unbiased way, of the dependence of the coordination environment of cations with intermediate structural role from the glass composition. Indeed, in the framework of the shell model potentials, the available libraries in the literature are based on atoms usually bearing full formal charges (Si^{4+}, P^{5+}, Al^{3+}, etc.) and it is well-known that to reproduce well the short-range order of network former tetrahedrally coordinated cations such as Si, P, and Al, the employment of three-body interatomic potentials is needed.[25,35,36] Instead, the rigid ionic potential with partial charges does not require the introduction of three-body terms and is therefore preferred when the aim of the study is the effect of the composition on the coordination environment of intermediate cations, such as gallium and aluminum. Once we demonstrated that the gallium atoms are predominantly 4-fold coordinated in the glasses (vide infra), we resorted to shell-model molecular dynamics simulations to investigate the whole structure of the three glass compositions. The SM interatomic parameters and the functional forms employed are reported in Table 2. It is worth highlighting that, whereas the Si−O, P−O, Ca−O, Na−O, and Al−O parameters have been taken from the literature,[25,26,36] the Ga−O parameters have been fitted in this work by using the same procedure described before for the RI model.

The initial configurations were generated by placing randomly 5000 atoms in a cubic box with dimensions imposed by the experimental density (Table 3), and three simulations were carried out with different starting configurations. The systems were heated at high temperature and cooled down to room temperature by using the melt and quench protocols described in ref 38 for both the RI and SM simulations.

In the case of RI MD simulations, the system is heated at 6000 K, equilibrated for 100 ps, and subsequently cooled down continuously from 6000 to 300 K in 1140 ps with a nominal

dx.doi.org/10.1021/jp400721g | J. Phys. Chem. B 2013, 117, 4142−4150

Table 2. Shell Model Interatomic Potential: Analytic Functions and Parameters

	Buckingham, $Ae^{-r/\rho} - C/r^6$		
	A (eV)	ρ (Å)	C (eV Å^6)
O_s-O_s	22764.30	0.1490	27.88
$Si-O_s$	1283.91	0.32052	10.661580
$Ca-O_s$	2152.3566	0.309227	0.09944
$Na-O_s$	56465.3453	0.193931	0.0000
$P-O_s$	1120.09133	0.334772	0.0000
$Al-O_s$	1460.3000	0.299120	0.0000
$Ga-O_s$	951.96638	0.340917	0.0000
	three-body potential, $^1/_2k_b(\theta - \theta_0)^2 \exp(-[r_{12}/\rho + r_{13}/\rho])$		
	k_b (eV rad^{-2})	θ_0 (deg)	ρ (Å)
O−Si−O	100.0	109.47	1.0
O−Al−O	100.0	109.47	1.0
O−Ga−O	100.0	109.47	1.0
O−P−O	50.0	109.47	1.0
	core−shell potential, $^1/_2k_sr^2$		
	k_s (eV Å^{-2})	$Y(e)$	
O_c-O_s	74.92	−2.8482	

Table 3. Number of Atoms of Each Chemical Species in the Simulation Box and Density of the Glasses Studied

	Si	Na	Ca	P	Ga/Al	O	density (g/cm^3)
BG	912	962	532	102		3092	2.719
GBG	800	844	464	90	34	2706	2.747
ABG	800	844	464	90	34	2706	2.733

cooling rate of 5 K/ps. The temperature is decreased by 0.01 K every time step using the Berendsen thermostat with the time constant parameter for the frictional coefficient set to 0.4 ps.

Another 100 ps of equilibration at constant energy and 50 ps of data production is performed at 300 K. Integration of the equation of motion is performed using the Verlet leapfrog algorithm with a time step of 2 fs.

Instead, for the SM potential, the systems were heated and held at 3200 K for 100 ps in the NVT ensemble, ensuring a suitable melting of the samples. The liquids were then cooled to 300 K at a nominal cooling rate of −5 K/ps. The resulting glass structures were subjected to a final NVT trajectory of 200 ps. A time step of 0.2 fs, i.e., small enough to control the high frequency motion of the core−shell spring during MD simulations, has been used to integrate the leapfrog equation of motion.

Coulomb interactions are calculated by the Ewald summation method with a cutoff of 12 Å and an accuracy of 10^{-4} for both models, whereas short-range cutoff values of 5.5 and 7.5 Å have been used for the RI and SM potentials, respectively.

It is important to emphasize that the short time scale accessible to molecular dynamics simulations leads to the usage of a cooling rate which is several orders of magnitude higher than the typical experimental one. This is known to result in a glass transition temperature higher than the actual one. For example, in the case of SM simulations, Tilocca et al.,[25] by using similar cooling rates, estimated a T_g value of 1030 K for 45S5 Bioglass, whereas we have estimated a T_g of about 950 K by using the rigid ionic model (unpublished work). These are about 220 and 140 K higher than the experimental value.[44]

However, previous simulations carried out on binary and ternary systems showed that, despite the different T_g, a cooling rate around 10 K/ps yields converged and accurate structural properties,[45] and this is currently used on most MD studies of melt-derived glasses and bioglasses.[38,46]

In a previous work, we have shown that whereas the cooling rate does not affect short-range order it slightly affects the medium range order such as the Q^n distributions.[47] Unfortunately, because of the computational effort required, we cannot generate glasses with a cooling rate significantly slower (of at least 1 or 2 orders of magnitude) with respect to that generally employed and thus we cannot see appreciable improvement on the medium range structure of these glasses.

Each glass structure obtained by the MD simulations has been analyzed in terms of radial distribution functions, bond angle distribution functions, coordination number distributions (CN), Q^n distributions, bridging oxygen (BO) abundances, network connectivity (NC), and ion clustering.

RESULTS AND DISCUSSION

Validation of Ga−O Interatomic Potential Parameters.

The parameters of Si−O, Na−O, Ca−O, Al−O, and P−O pairs were previously validated, while a test of the reliability of the parametrization derived in this study for the Ga−O pairs is provided by the comparison of the structure of several Ga-containing crystal phases obtained from the simulation with the experimental one reported in the literature. The structural data of the crystals used for the validation of the Ga−O interatomic

Table 4. Structural Properties of Ga-Containing Silicate and Phosphate Crystals Computed with the RI Parameters Derived in This Work[a]

crystal phase	space group	a (Å)	b (Å)	c (Å)	V_t (Å^3)	$(V - V_t)/V_t$ (%)	Ga−O (Å)
$Ca_{12}Ga_8Si_{12}O_{48}$	*I A* 3 *D* (cubic)	12.05 (12.02)	12.05 (12.02)	12.05 (12.02)	1749 (1737)	0.7	2.01 [6] (1.97)
$K_{9.72}Ga_{9.72}Si_{26.28}O_{72}$	*P* 6/*M M M*	19.18 (18.58)	19.18 (19.18)	7.55 (7.49)	2406 (2239)	7.4	1.67 [4] (1.66)
$K_{10.224}Ga_{10.224}Si_{25.776}O_{72}$	*P* 6/*M M M*	19.20 (18.67)	19.20 (18.67)	7.55 (7.49)	2413 (2262)	6.7	1.68 [4] (1.67)
$Ga_3P_3O_{12}$	*P* 3_1 2 1 (hexag.)	5.18 (4.87)	5.18 (4.87)	11.46 (11.03)	267 (227)	17.5	1.83 [6] (1.85)
$Ga_2P_2O_8$	*C* 2 2 21 (orthor.)	7.75 (6.97)	7.75 (6.97)	7.75 (6.87)	466 (333)	39.3	1.83 [4] (1.79)
$NaGaSiO_4$	*P* 63 (hexag.)	8.82 (8.73)	8.82 (8.73)	8.29 (8.21)	559 (542)	3.2	1.82 [4] (1.89)
$Na_2Ga_2Si_4O_{12}$	*C* 1 2/*C* 1 (Monocl.)	9.58 (9.56)	8.66 (8.70)	5.33 (5.27)	420 (418)	0.6	2.01 [6] (1.99)
$NaCaGaSi_2O_7$	*P* −4 21 *m* (tetrag.)	7.74 (7.71)	7.74 (7.71)	5.14 (5.06)	308 (301)	2.4	1.82 [4] (1.82)
$K_2Ga_2Si_6O_{16}$	*C* 1 2/*M* 1 (monocl.)	8.08 (8.64)	13.61 (13.10)	7.30 (7.23)	719 (737)	−2.4	1.67 [4] (1.66)
$Na_{4.2}K_{1.8}Ga_6Si_6O_{24}$	*P* 63 (hexag.)	8.88 (8.82)	8.88 (8.82)	8.40 (8.38)	565 (574)	1.7	1.71 [4] (1.71)
$Sr_4Ga_8Si_8O_{32}$	*P* 1 21/*A* 1 (monocl.)	8.99 (9.00)	9.48 (9.48)	8.65 (8.40)	737 (717)	2.8	1.70 [4] (1.73)

[a]The experimental data are reported in parentheses.

dx.doi.org/10.1021/jp400721g | J. Phys. Chem. B 2013, 117, 4142−4150

Table 5. Structural Properties of Ga-Containing Silicate and Phosphate Crystals Computed with the SM Parameters Derived in This Work[a]

crystal phase	space group	a (Å)	b (Å)	c (Å)	V_t (Å^3)	$(V - V_t)/V_t$ (%)	Ga−O (Å)
$NaGaSiO_4$	P 63 (hexag.)	8.89 (8.73)	8.89 (8.73)	8.38 (8.21)	574 (542)	6.0	1.83 [4] (1.89)
$Na_2Ga_2Si_4O_{12}$	C 1 2/C 1 (monocl.)	9.49 (9.56)	8.71 (8.70)	5.27 (5.27)	419 (418)	0.3	2.00 [6][b] (1.99)
$NaCaGaSi_2O_7$	P −4 21 m (tetrag.)	7.91 (7.71)	7.91 (7.71)	5.04 (5.06)	315 (301)	4.9	1.84 [4] (1.82)
$Na_6Ga_6Si_6O_{24}$	P 63 (hexag.)	8.89 (8.73)	8.89 (8.73)	8.38 (8.21)	574 (542)	6.0	1.83 (1.89)

[a]The experimental data are reported in parentheses. [b]The three-body potential was not used in this case.

parameters are reported in Tables 4 and 5 for the RI and the SM potentials, respectively.

The new parametrization provides structural properties for gallium silicate crystals in very good agreement with the experimental data, whereas a great discrepancy for Ga-phosphate crystals can be observed. However, this was expected, since the parametrization procedure was performed using silicate and oxide crystals only.[39] However, in view of the low content of P_2O_5 with respect to SiO_2 in the bioactive glasses investigated in this work and since X-ray experiments on heat-treated samples do not show any propensity to form Ga-phosphate segregation domains, the low accuracy in the reproduction of phosphate crystal structure can be considered not to be detrimental for the simulation of the investigated glasses. Interestingly, the mean Ga−O bond length is well reproduced with our RI parameters both in tetrahedral (4) and octahedral (6) coordination.

The accuracy of the new parameters has also been tested on the reproduction of the glass network structure of a ternary sodium gallosilicate glass with composition 25%Na_2O·25%Ga_2O_3·50%SiO_2 in mol (named NGS hereafter) for which structural data were experimentally obtained through ^{17}O MAS NMR experiments.[17]

Table 6 reports the RI-MD, SM-MD, and NMR derived coordination number distributions for Ga and the bridging

Table 6. Comparison between Ga and Si Coordination Number Distribution and Bridging Oxygen Abundance (%) Determined Experimentally and Computationally for the NGS Glass System

	Ga coordination number distribution			Si coordination number distribution		
	3	4	5	6	3	4
RI-MD	1.3	98.2	0.6	0	0	100
SM-MD	0.0	96.9	3.1	0	0	100
Exp		100				100
	bridging oxygen abundance (%)					
	Ga−O−Ga		Ga−O−Si		Si−O−Si	
RI-MD	20.0		60.2		19.8	
SM-MD	21.8		64.3		13.9	
Exp	14.5		70.3		15.2	

oxygen (BO) abundances in terms of Si−O−Si, Si−O−Ga, and Ga−O−Ga bridges. These features are very well reproduced by both models, although the SM yields T−O−T population sites in better agreement with experiments. The reproducibility of the coordination number of ions classified as intermediate glass network, such as Ga, is very important because the structural behavior of these elements is strictly related to their coordination environment (that is, tetrahedral vs octahedral).[48] Therefore, we can conclude that both the RI and SM parameters are able to reproduce the structural features of Ga-silicate glasses and can be safely employed to study the Ga-containing bioactive glasses.

Short Range Order. The analysis of the cation−oxygen X−O (X = Si, P, Na, and Ca) radial distribution functions of the investigated glasses obtained by using both the SM and RI models shows that the general features around silicon and phosphorus are unchanged in the three compositions studied. Since the radial distribution functions of the original 45S5 Bioglass have already been reported in several papers, they will not be reported here.[25,26,49] The mean Si−O distance is in the range 1.58−1.60 Å independently on the glass composition in good agreement with previous MD simulations and experimental data on similar glass compositions.[38,46,50] The P−O mean bond distance is 1.51−1.52 Å for the RI and 1.55 Å for the SM potentials in agreement with previous MD investigations[42,47] but shorter with respect to the P−O experimental mean bond length (1.645 Å) found in the pure P_2O_5 glass[51] or the mean P−O bond length of 1.60 Å proposed in a recent neutron diffraction study of the 45S5 Bioglass.[50] However, it must be highlighted that a great uncertainty was associated with this value because of the difficulty in the fitting of the P−O pair distribution function (PDF) from the neutron diffraction total distribution functions, due to the small number of P−O bonds with respect to the Si−O ones.[50] Both Si and P are found in a perfect tetrahedral coordination independently on the glass composition.

The Na−O and Ca−O peak positions are at 2.37/2.35 (RI/SM) and 2.38/2.30 Å (RI/SM), in agreement with the range of values obtained by X-ray and neutron diffraction measurements for phosphate and soda-lime silicate glasses, and the PDFs do not show significant differences between the three glasses.

Both Na and Ca are enclosed in a pseudooctaedral coordination shell of about six oxygen atoms typical of modifier and/or charge compensator cations.

The Al−O pair distribution function shown in Figure 1 has a narrow first peak (fwhm = 0.12) with a mean bond distance of 1.76/1.74 Å (RI/SM), characteristic of ions in tetrahedral coordination, acting as network formers. This is in very good

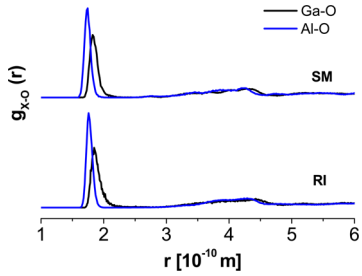

Figure 1. Ga−O and Al−O pair distribution functions obtained by using the RI (bottom) and SM (top) potentials for GBG and ABG glasses, respectively.

dx.doi.org/10.1021/jp400721g | J. Phys. Chem. B 2013, 117, 4142−4150

agreement with DFT calculations[35,52] and experimental distances measured in aluminosilicate glasses and crystalline analogous of different compositions for which the Al−O bond lengths range between 1.74 and 1.78 Å.[53−56]

In the RI simulations, only 0.5% of aluminum is present in 5-fold coordination, whereas no 6-fold coordinated aluminum atoms were detected; this seems not to be an artifact of the potential parameters employed, but it is most probably related to the very small percentage of aluminum (compared to silicon and modifier cation composition) contained in the investigated glass. In fact, Christie et al.[33] in a previous MD work making use of the same Al−O parameters found a non-negligible amount of 5- and 6-fold coordination sites in yttrium aluminosilicate glasses with a consistent amount of aluminum oxide. Moreover, several NMR experiments showed that the aluminum coordination strongly depends on the glass composition.[57] Instead, all the aluminum atoms are found in a 4-fold coordination when the SM potential is employed.

The shape of the first peak in the Ga−O PDF obtained by using the SM potential is broader (fwhm = 0.16 Å) than that of the Si−O (fwhm = 0.11 Å) and P−O (fwhm = 0.05 Å) ones and narrower than that of the Ca−O (fwhm = 0.26 Å) and Na−O (fwhm = 0.50 Å) PDFs. Thus, the Al coordination environment (fwhm = 0.12 Å) is more ordered than the Ga one.

The mean Ga−O bond length for the GBG glass is 1.86 Å with a CN of 4.5 when the RI model is used, whereas a bond distance of 1.83 Å with a CN of 4.1 is found with the SM potential. These results are in good agreement with a previous EXAFS structural study on $NaGaSi_3O_8$ glass for which the mean bond length for Ga−O was reported to be 1.88 Å with a predominant tetrahedral coordination (CN = 4.2). In the case of β-Ga_2O_3 where Ga ions are present both in tetrahedral and octrahedral sites, the mean Ga−O bond distances are 1.821 and 2.013 Å, respectively.[58]

The coordination environment is also unveiled by the O−X−O (X = Si, P, Al, Ga, Ca, and Na) bond angle distributions ($\rho(\theta)$) which are reported in Figures 2 and 3.

Figure 2 shows that the O−Si−O, O−P−O, and O−Al−O bond angle distributions are centered at 109° characteristic of network former ions in tetrahedral coordination independently on the glass compositions. Although the O−Al−O distribution is wider and noisier than the O−Si/P−O distributions, it does

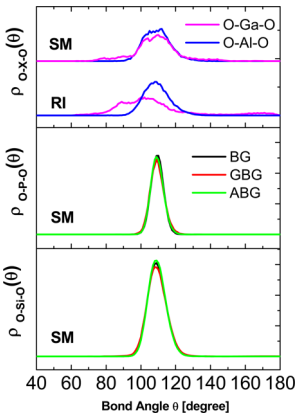

Figure 2. O−X−O bond angle distributions for BG, GBG, and ABG glasses. X = Si, P, Ga, and Al. The O−Al−O and O−Ga−O BADs obtained by using the RI potential model have also been reported.

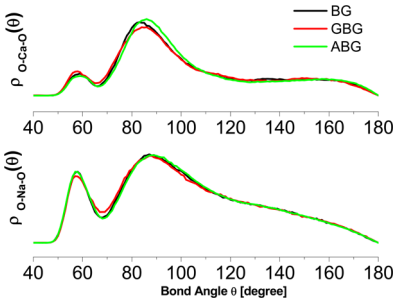

Figure 3. O−Ca−O and O−Na−O bond angle distributions obtained by using the SM potential model for BG, GBG, and ABG glasses.

not show other small peaks related to higher coordination numbers.

Some differences are detected for the O−Ga−O bond angle distribution when the RI model is used, in particular: (i) the distribution is considerably wider with respect to the O−Si−O, O−P−O, and O−Al−O ones; (ii) the distribution presents three quite evident peaks centered at around 90, 100, and 170° characteristic of 4-coordinated Ga ions with a high degree of disorder, and small amounts of 5- and 6-coordinated Ga ions.

Therefore, while Al plays a marked network former role in the ABG glass, Ga seems to have an intermediate role; in fact, while 62% of Ga is found in a tetrahedral coordination, the remaining 38% assumes a trigonal bypiramidal (29%) or octahedral (9%) coordination, as shown in Figure 4. A more ordered tetrahedral environment is found for the SM simulations; in this case, 88% of gallium atoms are in a tetrahedral coordination, while 12% are 5-fold coordinated.

Previous 3QMAS-NMR measurements on isocompositional gallo- and alluminosilicate glasses[17] showed a coordination environment slightly different for Ga and Al ions, the higher quadrupolar coupling constants of the various oxygens sites in gallosilicate glasses suggested a more disordered structure than that of aluminosilicate ones, and Ga ions showed a greater tendency to form coordination groups with more than four oxygens with respect to Al. This scenario is corroborated by the results of the MD simulations carried out in the present study that suggest a intermediate role for Ga and a pure network former role for Al.

These structural peculiarities can be the cause of the different solubility of ABG and GBG glasses in SBF observed experimentally. In fact, the $[GaO_4]^{-1}$ tetrahedra are bigger and bear a smaller charge density than the $[AlO_4]^{-1}$; they thus attract less efficiently the charge compensator Na and Ca ions[35,36] with a consequent increment of ionic leaching. The greater amount of ions released, in particular Ca ions, is the fundamental step for the bioactivity in terms of hydroxyapatite precipitation on the glass surfaces; conversely, the lower amount of Ca released in the case of ABG glasses in solution inhibits the hydroxyapatite formation, as reported in ref 59.

As already evidenced by the analysis of the radial and coordination number distributions, the O−Na−O and O−Ca−O bond angle distributions confirm that the environment around Na and Ca is not substantially changed upon addition of gallium and/or aluminum.

In fact, the O−Na−O and O−Ca−O bond angle distributions reported in Figure 3 show a peak close to 90°, which generally results from Na or Ca atoms in octahedral geometry connecting two NBOs belonging to different tetrahedra, while the second peak at 60° (more pronounced

dx.doi.org/10.1021/jp400721g | J. Phys. Chem. B 2013, 117, 4142−4150

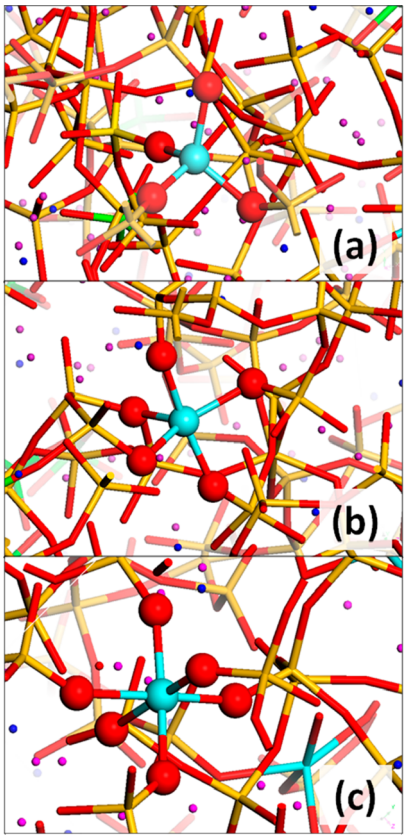

Figure 4. Types of coordination environments and relative quantity (%) of gallium species (cyan spheres) in the GBG glass obtained by using the RI model. Yellow and red sticks represent silicon and oxygen atoms, whereas magenta and blue spheres represent sodium and calcium, respectively.

for Na) results from modifiers coordinated to two NBOs (or one NBO and one BO) belonging to the same tetrahedron.[60]

Medium Range Order. The knowledge of the medium range structure of potential bioactive glasses has always been considered critical for predicting their chemical durability and bioactivity.[61] In this work, the medium range order has been characterized by considering the Q^n distributions of network former species as well as the bridge type distributions T−O−T (where T = Si, P, Al, and Ga). Only the results obtained by the SM potential are reported in Tables 7 and 8. The Q^n distributions, where n represents the number of bridging oxygens (BO) bonded to the network former ions, gives a measure of the glass network connectivity. The analysis has been performed on Si, P, Al, and the four-coordinated Ga atoms, that is, those acting as network formers. The bridge type distribution describes the type of connectivity between the network former ions. The connectivities considered (type of bridges) are Si−O−Si, P−O−P, Ga−O−Ga, Al−O−Al, Si−O−P, Si−O−Ga, Si−O−A, P−O−Al, and P−O−Ga.

The results show that the introduction of Ga or Al does not modify substantially the medium range order of the silicate network of the 45S5 Bioglass. The addition of Al or Ga causes a slight increase of the mean value of n for Q^n(Si) and Q^n(P) due to the formation of Si/P−O−Al and Si/P−O−Ga bridges, whereas the presence of a very small fraction of Al−O−Al and the absence of Ga−O−Ga bridges suggests a very low tendency of Al and Ga ions to aggregate in the GBG and ABG samples.

The structure of these glasses is composed by Q^2, Q^3, and Q^1 species. Phosphorus is predominantly present as Q^0 units (77−78%), but a non-negligible amount of Q^1 species (around 20%) is also detected.

Non-orthophosphate units are also detected in glass structural models generated by means of Car−Parrinello molecular dynamics simulations even though, due to the small box size usually employed in these studies, their amount does not have a reliable statistical value. On the experimental side, contradictory results have been reported in the past.[49,62,63] Recent high resolution ^{31}P MAS and static NMR investigations combined with DFT-NMR calculations of ^{31}P NMR parameters of the 45S5 Bioglass suggest the only presence of orthophosphate groups in the real sample,[21,50] while ^{31}P−^{29}Si REDOR experiments, performed on 99% ^{29}Si enriched 46.1SiO_2−51.3CaO-2.6P_2O_5 samples, reveal the presence of a very small quantity of PO_4 groups bonded to the silicate network through P−O−Si bridges.[64] Therefore, Ca-rich glasses seems to favor "unstable sites" like Si−O−P bonds probably because of the very low diffusivity of Ca caions.

Aluminum and gallium are both present as Q^4 species with a minor amount of Q^3 species. Table 7 also reports the network connectivity (NC) which is computed as weighted averages of the corresponding Q^n distributions. This is an important parameter for predicting bioactivity, since it has been shown that a threshold of NC = 3 separates bioactive from bioinactive compositions. High silica compositions with NC > 3 are usually more durable and less bioactive, whereas low-silica compositions with NC < 3 are usually less durable and bioactive.[46,65]

The NC(Si) slightly increases from 2.09 for BG to 2.15 for GBG and ABG glasses, and the same trend is seen for NC(P). Instead, the network connectivity of Al is higher than that of Ga and this leads to a more polymerized network for the ABG glass. In fact, the total network connectivity which accounts for all network former (Si and P) and intermediate ions (4-fold coordinated Al and Ga) increases from 1.90 for BG to 1.98 and 2.03 for GBG and ABG, respectively. These differences are very small, but they are significant considering the very small quantity of gallium and aluminum in the present glasses. On the basis of these results, Al-containing glasses should be less bioactive than Ga-containing bioactive glasses, in agreement with experimental evidence.

Table 7. Q^n Distribution and Bridging Type Distribution of the Different Species in the Glasses Studied[a]

	Q_{Si}^n						Q_P^n				Q_{Al}^n			$Q_{Ga}^{n\ b}$			
	Q^0	Q^1	Q^2	Q^3	Q^4	NC	Q^0	Q^1	Q^2	NC	Q^3	Q^4	NC	Q^3	Q^4	NC	NC_{TOT}
BG	0.9	17.3	54.0	27.4	0.4	2.09	78.4	19.6	2.0	0.24							1.90
GBG	0.3	16.4	54.2	26.3	2.8	2.15	77.6	19.6	2.8	0.25				7.1	80.8	3.4	1.98
ABG	0	14.7	57.8	25.3	2.2	2.15	77.8	22.2	0	0.22	14.3	85.7	3.9				2.03

[a]The data refer to the SM MD simulations (standard deviation of ±2−3% on the three simulations). [b]Both the Q^n species and the NC of Ga atoms have been normalized with respect to the number of four-coordinated Ga atoms.

dx.doi.org/10.1021/jp400721g | J. Phys. Chem. B 2013, 117, 4142−4150

Table 8. Bridging Type Distribution of the Different Species in the Glasses Studied[a]

	bridge type distribution								
	Si−O−Si	P−O−P	Al−O−Al	Ga−O−Ga	Si−O−P	Si−O−Al	Si−O−Ga	P−O−Al	P−O−Ga
BG	30.5	0.0			0.8				
GBG	28.3	0.0		0.0	0.6		5.0		0.2
ABG	28.6	0.0	0.1		0.5	4.5		0.2	

[a]The data refer to the SM MD simulations.

Ion Clustering. Previous MD simulations have suggested a possible correlation between the clustering of modifier cations and the chemical durability, since the tendency of the cations to aggregate in small clusters was observed to be more marked in bioactive glasses with more durable compositions.[33]

The ratio R_{X-Y} between the number of Y ions found around the X coordination sphere (N_{MD}) and the corresponding number that would result from a homogeneous distribution (N_{hom}) of the ions has been proposed as a statistical measure of the tendency of the X and Y cations to aggregate in the glass matrix:[33]

$$R_{X-Y} = \frac{N_{MD}}{N_{hom}} = \frac{CN_{X-Y}}{\frac{4}{3}\pi r_c^3 \frac{N_Y}{V_{Box}}}$$

where r_C and CN_{X-Y} are the distance of the first minimum in the X−Y PDF and the X−Y coordination number at that distance, whereas N_Y and V_{box} are the total number of Y atoms in the box and the total volume. Therefore, $R = 1$ indicates no clustering, while $R > 1$ implies spatial clustering.

The R_{XY} ratios for different X−Y pairs are reported in Table 9. The data show that the introduction of Al and Ga does not modify the tendency of aggregation of Na and Ca around Si, since the R_{Si-Na} and R_{Si-Ca} ratios are similar for the three glasses.

Table 9. Clustering Parameters (R_{X-Y}) for the SM Structural Models of the Three Glasses Studied

X−Y	BG	GBG	ABG
Si−Na	1.08	1.05	1.09
Si−Ca	1.12	1.15	1.11
P−Na	1.27	1.26	1.19
P−Ca	1.41	1.40	1.57
Si−Ga		1.49	
P−Ga		0.57	
Ga−Ga		0.00	
Si−Al			1.41
P−Al			0.57
Al−Al			1.14
Na−Na	1.26	1.18	1.21
Ca−Ca	1.16	1.27	1.27

In agreement with previous MD simulations on the 45S5 Bioglass, Na and Ca modifier ions prefer to coordinate phosphate groups with respect to the silicate ones, leading to a general increase in the polymerization of the silicate rich domains.[25,42,46] This effect is even more pronounced for GBG and ABG glasses. In fact, the R_{P-Ca} ratio increases from 1.40 for BG and GBG to 1.57 for ABG, suggesting the formation of more insoluble calcium phosphate segregation zones in the Al-containing bioactive glasses with respect to Ga containing bioactive glasses. An example of calcium phosphate rich regions containing six orthophosphate units found in the ABG glass is reported in Figure 5.

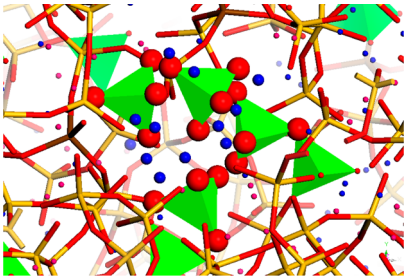

Figure 5. Example of the calcium phosphate domain found in the ABG glass. Phosphorus and oxygen atoms are represented in green tetrahedral and red balls, while calcium ions, in blue spheres.

It is worth noting that several experimental techniques can be employed to detect inhomogeneities and phase separation in silicate glasses.[66,67] Among these, high resolution electron microscopy has been extensively employed to investigate cation segregation in bioactive glasses,[68] in multicomponent ZnO−Na_2O−CaO−SiO_2 bioactive glasses,[69] and in ternary CaO−P_2O_5−SiO_2 glasses.[68] Instead, very recently nanometric-sized phosphate clusters in Na-free bioactive glasses have been revealed by solid-state ^{31}P NMR experiments by Fayon et al.[64] in nice agreement with molecular dynamics predictions.[46]

Table 9 also reports the R_{Na-Na} and R_{Ca-Ca} ratios which measure the tendency of self-aggregation between the modifier cations. This was also demonstrated to be correlated to the bioactivity of phosphosilicate glasses with increased silica content.[25] The tendency of self-aggregation is constant for Na cations in the three glasses, whereas it shows a slight increase for Ca cations in the ABG glass with respect to the BG and GBG glasses. However, as expected, the enhancement is small due to the very similar compositions of BG and ABG glasses. Another interesting difference between GBG and ABG glasses can be inferred by looking at the R_{Ga-Ga} and R_{Al-Al} ratios which reveal the higher tendency of Al ions to aggregate in the ABG glass with respect to Ga ions in the GBG sample for which Ga−Ga self-aggregation is not observed. Therefore, the formation of aluminum oxide segregation zones in the ABG glass could further explain its higher durability and bioinactivity.

CONCLUSIONS

The results of classical MD simulations used in this study to investigate the structural changes caused by the incorporation of Ga and Al ions in phosphosilicate bioactive glasses reveal that the short-range environment around Al is more ordered than that of Ga, and it is characteristic of a network former role; on the other hand, although Ga is predominantly found in 4-fold coordination, a minor fraction of atoms surrounded by five oxygens is also present; this results in a slightly less polymerized

dx.doi.org/10.1021/jp400721g | J. Phys. Chem. B 2013, 117, 4142−4150

network of Ga-containing glasses with respect to those doped with Al, and thus to a easier degradability of the former compositions.

When added in small quantities, Ga or Al ions do not change drastically the medium range order characteristic of the 45S5 Bioglass. However, the clustering of Ca ions around phosphorus is more pronounced passing from the BG and GBG to the ABG glass. The formation of insoluble calcium phosphate domains leads to more durable glasses and together with the enhanced clustering of Ca ions observed for GBG and ABG seems to emerge as a marker of nonbioactive behavior. Moreover, our simulations show that, while Al ions tend to self-aggregate in the ABG glass, Ga ions do not form gallium oxide segregation zones in the GBG glass.

In other words, the formation of inhomogeneous regions seems to inhibit the bioactive response of aluminum containing bioactive glasses; a possible explanation is that the mobility of phosphate groups associated with calcium ions in these local domains is reduced; as a consequence, the kinetics of release to the solution is negatively affected with respect to the bioactive compositions in which isolated phosphates are embedded in a uniform environment.[25,32]

AUTHOR INFORMATION

Corresponding Author

*E-mail: alfonso.pedone@unimo.it. Phone: +39 059 2055043. Fax: +39 059 3735.

Notes

The authors declare no competing financial interest.

REFERENCES

(1) Hench, L. L.; Splinter, R. J.; Allen, W.-C.; Greenle, T. Mechanisms of Interfacial Bonding between Ceramics and Bone. *J. Biomed. Mater. Res. Symp.* **1971**, *2*, 117−141.

(2) Perez-Pariente, J. B., F.; Roman, J.; Salinas, A. J.; Vallet-Regi, M. Influence of Composition and Surface Characteristics on the In Vitro Bioactivity of SiO_2-CaO-P_2O_5-MgO Sol-Gel Glasses. *J. Biomed. Mater. Res.* **1999**, *47*, 170−175.

(3) Bini, M. G., S.; Capsoni, D.; Mustarelli, P.; Saino, E.; Visai, L. SiO_2-P_2O_5-CaO Glasses and Glass-Ceramics with and without ZnO: Relationships among Composition, Microstructure, and Bioactivity. *J. Phys. Chem. C* **2009**, *113*, 8821−8828.

(4) Verne, E. F., S.; Miola, M.; Fucale, G.; Maina, G.; Martinasso, G.; Canuto, R. A.; Di Nunzio, S.; Vitale-Brovarone, C. Synthesis and Characterisation of Bioactive and Antibacterial Glass-Ceramic Part 2-Plasma Spray Coatings on Metallic Substrates. *Adv. Appl. Ceram.* **2008**, *107*, 234−244.

(5) Lusvardi, G. M., G.; Menabue, L.; Menziani, M. C.; Pedone, A.; Segre, U.; Aina, V.; Petardi, A.; Morterra, C.; Boccafoschi, F.; Gatti, S.; Borsetti, M.; Cannas, M. Properties of Zinc Releasing Surfaces for Clinical Applications. *J. Biomater. Appl.* **2008**, *22*, 505−526.

(6) Salinas, A. J.; Shruti, S.; Malavasi, G.; Menabue, L.; Vallet-Regi, M. Substitutions of Cerium, Gallium and Zinc in Ordered Mesoporous Bioactive Glasses. *Acta Biomater.* **2011**, *7*, 3452−3458.

(7) Aina, V.; Marchis, T.; Laurenti, E.; Diana, E.; Lusvardi, G.; Malavasi, G.; Menabue, L.; Cerrato, G.; Morterra, C. Functionalization of Sol Gel Bioactive Glasses Carrying Au Nanoparticles: Selective Au Affinity for Amino and Thiol Ligand Groups. *Langmuir* **2010**, *26*, 18600−18605.

(8) Bernstein, L. R. Mechanisms of Therapeutic Activity for Gallium. *Pharmacol. Rev.* **1998**, *50*, 665−682.

(9) Valappil, S. P.; Ready, D.; Abou Neel, E. A.; Pickup, D. M.; O'Dell, L. A.; Chrzanowski, W.; Pratten, J.; Newport, R. J.; Smith, M. E.; Wilson, M.; Knowles, J. C. Controlled Delivery of Antimicrobial Gallium Ions from Phosphate-Based Glasses. *Acta Biomater.* **2009**, *5*, 1198−1210.

(10) Abou Neela, E. A.; Ahmeda, I.; Prattenb, J.; Nazhata, S. N.; Knowles, J. C. Characterisation of Antibacterial Copper Releasing Degradable Phosphate Glass Fibres. *Biomaterials* **2005**, *26*, 2247.

(11) Mouriño, V.; Newby, P.; Boccaccini, A. R. Preparation and Characterization of Gallium Releasing 3-D Alginate Coated 45S5 Bioglass (R) Based Scaffolds for Bone Tissue Engineering. *Adv. Eng. Mater.* **2010**, *12*, B283−B289.

(12) Franchini, M.; Lusvardi, G.; Malavasi, G.; Menabue, L. Gallium-Containing Phospho-Silicate Glasses: Synthesis and In Vitro Bioactivity. *Mater. Sci. Eng., C* **2012**, *32*, 1401−1406.

(13) Shruti, S.; Salinas, A. J.; Malavasi, G.; Lusvardi, G.; Menabue, L.; Ferrara, C.; Mustarelli, P.; Vallet-Regi, M. Structural and In Vitro Study of Cerium, Gallium and Zinc Containing So-Gel Bioactive Glasses. *J. Mater. Chem.* **2012**, *22*, 13698−13706.

(14) Senderov, E. E.; Vasiliev, N. S.; Yudin, E. I. The Order-Disorder Transition in Gallium Analog of Albite, $NaGaSi_3O_8$. *Phys. Chem. Miner.* **1982**, *8*, 51−54.

(15) Åhman, J.; Svensson, G.; Albertsson, J. A Reinvestigation of Beta-Gallium Oxide. *Acta Crystallogr., Sect. C* **1996**, *C52*, 1336−1338.

(16) Stebbins, J. F.; Xu, Z. NMR Evidence for Excess Non-Bridging Oxygen in an Aluminosilicate Glass. *Nature* **1997**, *390*, 60−62.

(17) Peng, L.; Stebbins, J. F. High Resolution O-17 MAS and Triple-Quantum MAS NMR Studies of Gallosilicate Glasses. *J. Non-Cryst. Solids* **2008**, *354*, 3120−3128.

(18) Hench, L. L. Bioceramics, a Clinical Success. *J. Am. Ceram. Soc.* **1998**, *81*, 1705−1728.

(19) Andersson, H.; Liu, G.; Karlsson, K. H.; Niemi, L.; Miettinen, J.; Juhanoja, J. In Vivo Behaviour of Glasses in the SiO_2-CaO-Al_2O_3-Na_2O-B_2O_3-P_2O_5 System. *J. Mater. Sci. Mater. Med.* **1990**, *1*, 219−227.

(20) Greenspan, H. D. C.; Hench, L. L. Mechanical-Behavior of Bioglass Coated Alumina. *J. Biomed. Mater. Res.* **1976**, *10*, 503−509.

(21) Pedone, A.; Charpentier, T.; Malavasi, G.; Menziani, M. C. New Insights into the Atomic Structure of 45S5 Bioglass by Means of Solid-State NMR Spectroscopy and Accurate First-Principles Simulations. *Chem. Mater.* **2010**, *22*, 5644−5652.

(22) Corno, M.; Pedone, A. Vibrational Features of Phospho-Silicate Glasses: Periodic B3LYP Simulations. *Chem. Phys. Lett.* **2009**, *476*, 218−222.

(23) Corno, M.; Pedone, A.; Dovesi, R.; Ugliengo, P. B3LYP Simulation of the Full Vibrational Spectrum of 45S5 Bioactive Silicate Glass Compared to *v*-Silica. *Chem. Mater.* **2008**, *20*, 5610−5621.

(24) Du, J.; Xiang, Y. Effect of Strontium Substitution on the Structure, Ionic Diffusion and Dynamic Properties of 45S5 Bioactive Glasses. *J. Non-Cryst. Solids* **2012**, *358*, 1059−1071.

(25) Tilocca, A.; Cormack, A. N.; De Leeuw, N. H. The Structure of Bioactive Silicate Glasses: New Insight from Molecular Dynamics Simulations. *Chem. Mater.* **2007**, *19*, 95−103.

(26) Pedone, A.; Malavasi, G.; Menziani, M. C. Computational Insight into the Effect of CaO/MgO Substitutions on the Structural Properties of Phospho-Silicate Bioactive Glasses. *J. Phys. Chem. C* **2009**, *113*, 15723−15730.

(27) Pedone, A.; Charpentier, T.; Menziani, M. C. The Structure of Fluorine-Containing Bioactive Glasses: New Insights from First-Principles Calculations and Solid State NMR Spectroscopy. *J. Mater. Chem.* **2012**, *22*, 12599−12608.

(28) Christie, J. K.; Pedone, A.; Menziani, M. C.; Tilocca, A. Fluorine Environment in Bioactive Glasses: Ab Initio Molecular Dynamics Simulations. *J. Phys. Chem. B* **2011**, *115*, 2038−2045.

(29) Mead, R. N.; Mountjoy, G. Modeling the Local Atomic Structure of Bioactive Sol-Gel Derived Calcium Silicates. *Chem. Mater.* **2006**, *18*, 3956−3964.

(30) Mead, R. N.; Mountjoy, G. A Molecular Dynamics Study of the Atomic Structure of $(CaO)x(SiO_2)_{1-x}$ Glasses. *J. Phys. Chem. B* **2006**, *110*, 14273−14278.

(31) Xiang, Y.; Du, J. Effect of Strontium Substitution on the Structure of 45S5 Bioglasses. *Chem. Mater.* **2011**, *23*, 2703−2717.

(32) Tilocca, A.; Cormack, A. N. Structural Effects of Phosphorus Inclusion in Bioactive Silicate Glasses. *J. Phys. Chem. B* **2007**, *111*, 14256−14264.

(33) Christie, J. K.; Tilocca, A. Aluminosilicate Glasses As Yttrium Vectors for in situ Radiotherapy: Understanding Composition-Durability Effects through Molecular Dynamics Simulations. *Chem. Mater.* **2010**, *22*, 3725−3734.
(34) Du, J. Molecular Dynamics Simulations of the Structure and Properties of Low Silica Yttrium Aluminosilicate Glasses. *J. Am. Ceram. Soc.* **2009**, *92*, 87−95.
(35) Pedone, A.; Gambuzzi, E.; Malavasi, G.; Menziani, M. C. First-Principles Simulations of the ^{27}Al and ^{17}O Solid State NMR Spectra of the $CaAl_2Si_3O_{10}$ Glass. *Theor. Chem. Acc.* **2012**, *131*, 1147−1157.
(36) Pedone, A.; Gambuzzi, E.; Menziani, M. C. Unambigous Description of the Oxygen Environment in Multicomponent Aluminosilicate Glasses from O-17 Solid State NMR Computational Spectroscopy. *J. Phys. Chem. C* **2012**, *115*, 14599−14609.
(37) Smith, W.; Forester, T. R. DL_POLY_2.0: A General-Purpose Parallel Molecular Dynamics Simulation Package. *J. Mol. Graphics* **1996**, *14*, 136−141.
(38) Pedone, A. Properties Calculations of Silica-Based Glasses by Atomistic Simulations Techniques: A Review. *J. Phys. Chem. C* **2009**, *113*, 20773−20784.
(39) Pedone, A.; Malavasi, G.; Menziani, M. C.; Cormack, A. N.; Segre, U. A New Self-Consistent Empirical Interatomic Potential Model for Oxides, Silicates, and Silica Based Glasses. *J. Phys. Chem. B* **2006**, *110*, 11780−11795.
(40) Ori, G.; Montorsi, M.; Pedone, A.; Siligardi, C. Insight into the Structure of Vanadium Containing Glasses: A Molecular Dynamics Study. *J. Non-Cryst. Solids* **2011**, *357*, 2571−2579.
(41) Gale, J. D.; Rohl, A. L. The General Utilty Lattice Program (GULP). *Mol. Simul.* **2003**, *29*, 291−341.
(42) Lusvardi, G.; Malavasi, G.; Menabue, L.; Menziani, M. C.; Pedone, A.; Segre, U. A Computational Tool for the Prediction of Crystalline Phases Obtained from Controlled Crystallization of Glasses. *J. Phys. Chem. B* **2005**, *109*, 21586−21592.
(43) Tilocca, A. Short- and Medium-Range Structure of Multicomponent Bioactive Glasses and Melts: An Assessment of the Performances of Shell-Model and Rigid-Ionic Potentials. *J. Chem. Phys.* **2008**, *129*, 084504.
(44) Hench, L. L.; Andersson, O. H. Bioactive Glasses. In *An Introduction to Bioceramics*; World Scientific: Singapore, 1993.
(45) Vollmayr, K.; Kob, W.; Binder, K. Cooling-rate Effects in Amorphous Silica: A Computer-Simulation Study. *Phys. Rev. B* **1996**, *54*, 15808−15827.
(46) Tilocca, A. Structural Models of Bioactive Glasses from Molecular Dynamics Simulations. *Proc. R. Soc. London, Ser. A* **2009**, *465*, 1003−1027.
(47) Pota, M.; Pedone, A.; Malavasi, G.; Durante, C.; Cocchi, M.; Menziani, M. C. Molecular Dynamics Simulations of Sodium Silicate Glasses: Optimization and Limits of the Computational Procedure. *Comput. Mater. Sci.* **2010**, *47*, 739−751.
(48) Shelby, J. S. *Introduction to Glass and Technology*; The Royal Society of Chemistry: Cambridge, U.K., 1997.
(49) Linati, L.; Lusvardi, G.; Malavasi, G.; Menabue, L.; Menziani, M. C.; Mustarelli, P.; Pedone, A.; Segre, U. Medium Range Order in Phospho-Silicate Bioactive Glasses: Insights from MAS-NMR Spectra, Chemical Durability Experiments and Molecular Dynamics Simulations. *J. Non-Cryst. Solids* **2008**, *354*, 84−89.
(50) Martin, R. A.; Twyman, H. L.; Rees, G. J.; Smith, J. M.; Barney, E. R.; Smith, M. E.; Hanna, J. V.; Newport, R. J. A Structural Investigation of the Alkali Metal Site Distribution within Bioactive Glass Using Neutron Diffraction and Multinuclear Solid State NMR. *Phys. Chem. Chem. Phys.* **2012**, *14*, 12105−12113.
(51) Martin, S. W. Review of the Structures of Phosphate Glasses. *Eur. J. Solid State Inorg. Chem.* **1991**, *28*, 163−205.
(52) Benoit, M.; Profeta, M.; Mauri, F.; Pickard, C. J.; Tuckerman, M. E. First-Principles Calculation of the O-17 NMR Parameters of a Calcium Aluminosilicate Glass. *J. Phys. Chem. B* **2005**, *109*, 6052−6060.
(53) Taylor, M.; Brown, G. E. Structure of Mineral Glasses. 1. Feldspar Glasses $NaAlSi_3O_8$, $KAlSi_3O_8$, $CaAl_2Si_2O_8$. *Geochim. Cosmochim. Acta* **1979**, *43*, 61−77.
(54) Himmel, B.; Wigelt, J.; Gerber, T.; Nofz, M. Structure of Calcium Aluminosilicate Glasses -Wide-Angle X-Ray Scattering and Computer-Simulation. *J. Non-Cryst. Solids* **1991**, *136*, 27−37.
(55) Petkov, V.; Gerber, T.; Himmel, B. Atomic Ordering in $Ca_{x/2}Al_xSi_{1-x}O_2$ Glasses (x=0,0.34,0.5,0.68) by Energy-Dispersive X-ray Diffraction. *Phys. Rev. B* **1998**, *58*, 11982−11989.
(56) Petkov, V.; Billinger, S. J. L.; Shastri, S. D.; Himmel, B. Polyhedral Units and Network Connectivity in Calcium Aluminosilicate Glasses from High-Energy X-Ray Diffraction. *Phys. Rev. Lett.* **2000**, *85*, 3436−3439.
(57) Neuville, D. R.; Cormier, L.; Massiot, D. Al Coordination and Speciation in Calcium Aluminosilicate Glasses: Effects of Composition Determined by ^{27}Al MQ-MAS NMR and Raman Spectroscopy. *Chem. Geol.* **2006**, *229*, 173−185.
(58) Okuno, M.; Marumo, F.; Sakamak, T.; Hosoya, S.; Miyake, M. The Structure Analyses of $NaGaSi_3O_8$, $NaAlGe_3O_8$ and $NaGaGe_3O_8$ Glasses by X-Ray Diffraction and EXAFS Measurements. *Miner. J.* **1984**, *12*, 101−121.
(59) Ohtsuki, C.; Kokubo, T.; Yamamuro, T. Mechanism of Apatite Formation on $CaO-SiO_2-P_2O_5$ Glasses in a Simulated Body-Fluid. *J. Mater. Sci. Mater. Med.* **1992**, *3*, 119−125.
(60) Tilocca, A.; de Leeuw, N. H. Ab Initio Molecular Dynamics Study of 45S5 Bioactive Silicate Glass. *J. Phys. Chem. B* **2006**, *110*, 25810−25816.
(61) Tilocca, A.; Cormack, A. N.; de Leeuw, N. The Structure of Bioactive Silicate Glasses: New Insight from Molecular Dynamics Simulations. *Chem. Mater.* **2007**, *19*, 95.
(62) Clayden, N. J.; Pernice, P.; Aronne, A. Multinuclear NMR Study of Phosphosilicate Gels Derived from $POCl_3$ and $Si(OC_2H_5)_4$. *J. Non-Cryst. Solids* **2005**, *351*, 195−202.
(63) Lin, C. C.; Huang, L. C.; Shen, P. $Na_2CaSi_2O_6-P_2O_5$ Based Bioactive Glasses. Part 1: Elasticity and Structure. *J. Non-Cryst. Solids* **2005**, *351*, 3195−3203.
(64) Fayon, F.; Duée, C.; Poumeyrol, T.; Allix, M.; Massiot, D. Evidence of Nanometric-Sized Phosphate Clusters in Bioactive Glasses as Revealed by Solid-State ^{31}P NMR. *J. Phys. Chem. C* **2013**, *117*, 2283−2288.
(65) Strnad, Z. Role of the Glass Phase in Bioactive Glass-Ceramics. *Biomaterials* **1992**, *13*, 317−321.
(66) Elmer, T. H.; Nordberg, M. E.; Carrier, G. B.; Korda, E. J. Phase Separation in Borosilicate Glasses as Seen by Electron Microscopy and Scanning Electron Microscopy. *J. Am. Ceram. Soc.* **1970**, *53*, 171−175.
(67) Sen, S.; Stebbins, J. F. Phase Separation, Clustering, and Fractal Characteristics in Glass: A Magic-Angle-Spinning NMR Spin-Lattice Relaxation Study. *Phys. Rev. B* **1994**, *50*, 822−830.
(68) Vallet-Regi, M.; Salinas, A. J.; Ramìrez-Castellanos, J.; Gonzáles-Calbet, J. M. Nanostructure of Bioactive Sol-Gel Glasses and Organic Anorganic Hybrids. *Chem. Mater.* **2005**, *17*, 1874−1879.
(69) Malavasi, G.; Lusvardi, G.; Pedone, A.; Menziani, M. C.; Dappiaggi, M.; Gualtieri, A.; Menabue, L. Crystallization Kinetics of Bioactive Glasses in the $ZnO-Na_2O-CaO-SiO_2$ System. *J. Chem. Phys. A* **2007**, *111*, 8401−8408.